Phthalocyanoiron Complex with Bridged Ligands. Electronic Structure of Monomers and Polymers

FERNANDO MENDIZABAL,[1] CLAUDIO OLEA-AZAR,[2] RODOLFO BRIONES[2]

[1]*Departamento de Química, Facultad de Ciencias, Universidad de Chile, Casilla 653, Santiago, Chile*
[2]*Departamento de Química Inorgánica y Analitica, Facultad de Ciencias Químicas y Farmacéuticas, Universidad de Chile, Casilla 233, Santiago 1, Chile*

ABSTRACT: Electronic structure aspects related to the semiconducting properties of monomers and polymers of phthalocyanoiron with bidentate bridging ligands, PcFe–L_2 and —[PcFe(L)]$_n$, have been investigated from density functional calculations [L = pyrazine, triazine, tetrazine, pyridine, 4,4′-bipyridine, bipyridyacetylene, and bis(4-pyridyl)bencene]. The following relevant results have been obtained: (a) an energy analysis in terms of electrostatic interaction, Pauli repulsion, and occupied/virtual orbital interactions show that the Pauli repulsion is the origin that the axial ligands (L) prefer be located toward the aza positions of the macrocycle, and (b) the intrinsic semiconducting properties depend of the frontier band. The valence band is composed largely by the transition metal d_{xy} orbital. The conduction band is composed of a mixture between the metallomacrocycle and bridged ligand orbitals for systems formed by pyrazine, bipyridine, and bipyridyacetylene. However, this composition is different when the ligands are triazine and tetrazine, which show a band composed of π^* orbitals. These systems are predicted to show the higher conductivity within the series, in agreement with experimental results. c

Key words: phthalocyanoiron complexes and polymers; electronic properties; density functional calculations

Correspondence to: F. Mendizabal; e-mail: hagua@abello.dic.uchile.cl.

Contract grant sponsor: FONDECYT.
Contract grant number: 1990038.

Introduction

Bridged quasi-one-dimensional metallomacrocycle complexes linked by linear bridging ligand (L) —[MacM(L)]$_n$ have been rather recently synthesized [1–14]. They have been classified as "shish-kebab polymers." Macrocycles of the phathalocyanine (Pc) type, tetrabenzoporphyrine (TBP), 1,2- and 2,3-naphthalocyanine (1,2- and 2,3-Nc), and others have been used. Fe, Ru, Os, Co, and other metals were taken as central metals. The bridging ligands (L) are linear π-electron-containing organic molecules bonded to the metal atom. For example, pyrazine (pyz), triazine (tri), tetrazine (tz), 4,4′-bipyridine (bpy), bipyridyacetylene (bpyac), *p*-diisocynobenzene (dib), tetrachlrodiisocyanobenzene (Cl_4dib), diisocyanobiphenyl (dibph), etc., have been used.

Metallophthalocyanines have been mainly investigated as part of efforts to construct new types of low-dimensional compounds [15–27]. The central metal (M) and the bridging ligand can be changed systematically. The stacking is achieved biaxially connecting the central transition metal with the bidentate bridging ligands (L).

The physical properties displayed by these systems have attracted much attention [28, 29]. This type of polymers shows a high technological interest due to their comparatively high thermal stability and their good semiconducting properties [30–34]. Furthermore, the bridged transition metal compounds are of special interest because they re ones few stable polymers that exhibit intrinsic conductivities, without external oxidative doping. One of the factors responsible of the electrical conductivity in these complexes is the band gap, which may be approximated as the energy difference between the lowest unoccupied molecular orbital (LUMO) and highest occupied molecular orbital (HOMO). The experimental values of the band gaps are between 0.1 and 1.5 eV [8–14]. Interesting magnetic, nonlinear optic, and photoconductivity properties also have been observed in some of these compounds [35–37]. In general, the structural variety of these polymers stimulates a study of the physical properties and develops new semiconducting materials.

Theoretical studies of —[MacFe(L)]$_n$, with L = pyz, C_2^{-2}, CN^-, where Mac is a reduced macrocycle as tetraazaporphyrine (TAP), has been studied by the tight-binding method based upon the extended Hückel formalism [38–40]. In these studies, a semiconducting behavior of the systems such as —[TAPFe(pyz)]$_n$ was predicted. The band gap is mostly determined by the difference between the LUMO of the bridging ligand and the HOMO transition metal d_{xy}. However, the use of some reduced models to describe properties of semiconduction for real systems may be somehow different, since the conduction band is formed between the bridging ligand and the macrocycle. Furthermore, intrinsic semiconductor is characterized by a small band gap and a lower density of highly mobile intrinsic charge carriers, it is necessary to use a more real model like the phthalocyaninato dianion.

In this work, the electronic structure of a series of PcFe(L)$_2$ complexes and —[PcFe(L)]$_n$ polymers are investigated in detail through the density functional approach, with special emphasis on the study of the metal–bridged ligand interactions. We try to answer some questions concerning the electronic properties the complexes, such as: (i) Why is the plane of the bridged ligand perpendicular to the phathalocyanine core, passing through the aza position of the macrocycle? (ii) Which is the nature and the magnitude of the band gap HOMO–LUMO? (iii) What is the relationship between the structural and electronic features of bridged ligands and their semiconducting properties? According to previous results, the LUMO would be formed by the bridging ligand and HOMO by the transition metal of metallomacrocycle. Therefore, to achieve semiconducting properties in such systems, the metallomacrocycle should contain a high-lying HOMO and the bridging ligand has a low-lying LUMO. The study of the electronic structure of this family of compounds may help to rationalize the effects of several factors in the conducting properties of these materials.

To answer these and others questions, we have used an energy decomposition scheme (see the discussion in the following section) that combined with a fragment formalism, has proved to be a useful tool in the analysis of PcFe–bridged ligand interactions. This scheme allows us to separate the steric factors from the attractive orbital interaction contributions. Figures 1–3 show the PcFe complex, the polymers, and the bridged ligands, respectively.

Computational Details and Geometrical Parameters

We used the Amsterdam Density Functional [41, 42] (ADF 2.3 version) program package, based in the LCAO density functional for the complexes

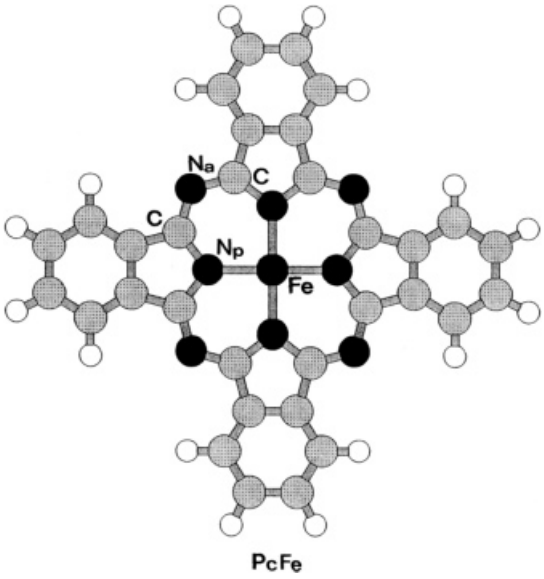

FIGURE 1. Phthalocyanoiron, PcFe.

and polymers (ADF-band 1.0 version) [43]. Bonding energies were evaluated by the generalized transition-state method. We have included Becke's nonlocal correction [44] to the local HFS exchange energy [local density approximation (LDA)] as well as Stoll's correction [45] for correlation between electrons of different spins, based on Vosko et al. parametrization [46] from electron gas data. This Hamiltonian has demonstrated to give an excellent description of systems with metallomacrocycles [47–49].

Moreover, for the calculation on the polymers, we used the ADF band code at the LDA level of theory and nonlocal gradient corrections by Becke for the exchange energy. On a more technical field, all the calculations were performed with an integration accuracy greater than 10^{-4} and at 10 *k*-points in the reduced Brillouin zone for all the one-dimensional (1D) cells.

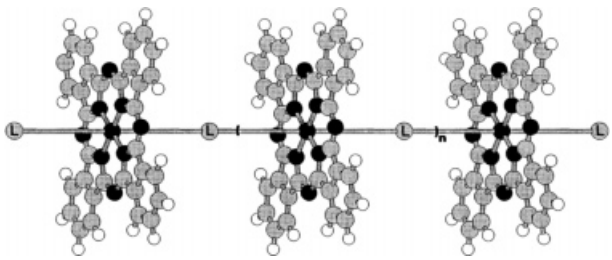

FIGURE 2. Structures of the metallomacrocycle polymers and their related complexes.

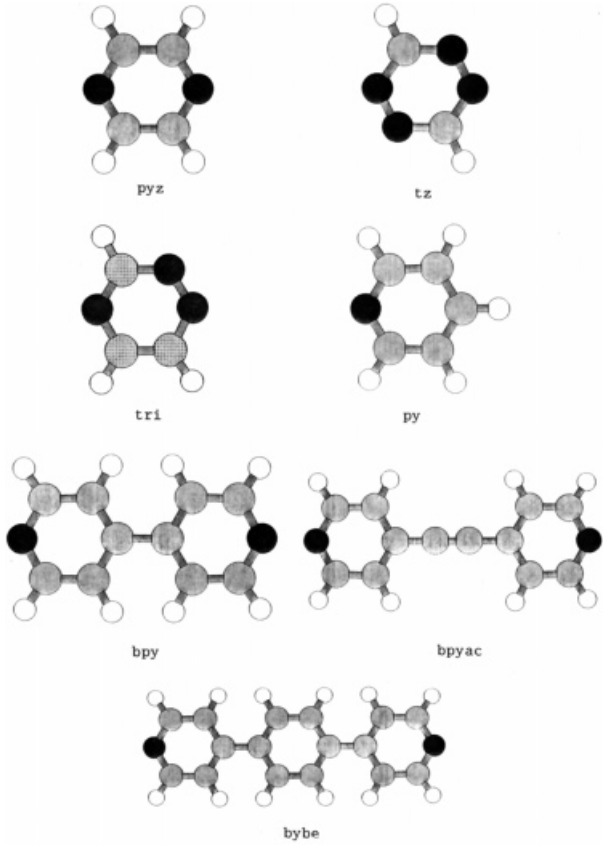

FIGURE 3. Bridged ligands (L): pyz, tri, tz, py, bpy, bpyac, and bybe.

The molecular orbitals were expanded in an uncontracted double-ξ Slater-type orbital (STO) basis set [50] for all atoms with the exception of the transition metal (Fe) orbitals, for which we used a triple-ξ basis set. As polarization functions one 4*p* STO was used for Fe. The cores (Fe: 1*s*-2*p*; C, N = 1*s*) were kept frozen [41, 42]. For the polymers, we used a basis set of numerical atomic orbital (NAOs) obtained from the STOs for each atom.

In order to analyze the interactions between FePc and two bridged ligand molecules (L) in the complexes, we decomposed the bonding energy into a number of terms, using the scheme of Morokuma [51]. The binding energy, ΔE, is obtained from the difference between the complex and the fragments:

$$\Delta E = E^{\mathrm{PcFe(L)_2}} - E^{\mathrm{PcFe}} - E^{(\mathrm{L})_2}. \qquad (1)$$

The binding energy can be decomposed in two terms,

$$\Delta E = \Delta E^0 + \Delta E_{0i}. \qquad (2)$$

The first term, ΔE^0, is called the steric repulsion [52, 53], which may be splitted at the same time in two components: (i) the electrostatic interaction ΔE_{elstat} of the nuclear charges and unmodified electronic charge density of one fragment with those of the other fragment. Both fragments are at their final positions. Usually ΔE_{elstat} is negative, i.e., stabilizing. (ii) The other component is the exchange repulsion or Pauli repulsion ΔE_{Pauli} [54, 55]. This is due to the antisymmetric requirement on the total wave function. It could be understood in a one-electron model as arising from the two-ortibal four-(three-)electron destabilizing interactions between occupied orbitals on the fragments. The steric repulsion term ΔE^0 is usually repulsive at the equilibrium distance, since the repulsive component ΔE_{Pauli} dominates in that region.

The second term, ΔE_{0i}, comes from the mixing of virtual orbitals of the fragments with the occupied orbitals. This is called the electronic interaction energy [56].

We are also interested in estimating the conductivity properties of these systems. The Fermi level (ε_f) is a reference state separating the occupied and unoccupied electronic levels in a solid. This band gap plays an important role in solid-state physics. In the context of density functional theory (DFT) the band gap is the hardness η [57, 58]. This basic quantity is defined as [59]

$$\eta = \left(\frac{\partial^2 E}{\partial N^2}\right)_{\nu} = I - A, \tag{3}$$

where E is the electronic energy, N the number of electrons, ν the external potential, I the ionization potential, and A the electron affinity. Working definitions of the quantities I and A are possible within molecular theory [60, 61]. For instance, by using Koopmans theorem, the ionization potential and electron affinity may be approximated as $I \cong -\varepsilon_{\text{HOMO}}$ and $A \cong -\varepsilon_{\text{LUMO}}$ [62], respectively. With these approximations, the hardness becomes

$$\eta \cong \varepsilon_{\text{LUMO}} - \varepsilon_{\text{HOMO}}, \tag{4}$$

where $\varepsilon_{\text{HOMO}}$ is the energy of the highest occupied molecular orbital (HOMO) and $\varepsilon_{\text{LUMO}}$ is the energy of the lowest unoccupied molecular orbital (LUMO). For solids, η is the half of the band gap [63]. A bigger η means a large I and a smaller A, which implies that the system has a smaller tendency to accept electrons and/or a smaller tendency to give away electrons. Thus, hardness can be seen as a resistance to charge transfer [60, 61]. From an experimental point of view, the conductivity (σ) is proportional to $e^{-E_g/2kT}$ with T being the temperature and E_g the energy band gap. Thus, the conductivity (σ) of a semiconductor depends on the energy required to promote electrons from the Fermi level across the band gap (E_g) [64, 65]. We associate the magnitude of η with the property of semiconductivity in the systems [61].

We have first performed calculations on the FePc isolated molecule using the experimental geometry (X-ray data) [66], with appropriate averaging of bond angles and bond lengths to maintain the D_{4h} symmetry. The coordinate system used in the calculation is shown in Figure 1. The monomers have been built by linking PcFe (metallomacrocycle) with linear bidentate bridging ligands, metal over ligand, along the stacking direction (z axis in our coordinate system). In the Figure 2 is shown the molecular stack. We have used the bridging ligands: pyridine (py), pyrazine (pyz), triazine (tri), tetrazine (tz), 4,4′-bipyridine (byp), bipyridyacetylene (byac), and bis(4-pyridyl)bencene (bybe) (see Fig. 3). The bridged structure shown in Figure 2 has been confirmed for many compounds using a variety of physical methods [infrared (IR), Mössbauer spectroscopy, nuclear magnetic resonance (NMR), thermogravimetry, and scanning tunneling microscopy] [8–14, 67–70]. The crystal structures of very similar compounds TPPFe(Pyz)$_2$ (TPP = tetraphenylporphyrinato), PcCo(py)SCN, and [DMDCo(pyz)]$_n$ (DMG = dimethylglyoximate) [71–73] show that the pyrazine and pyridine molecules in monomer and chain are all arranged within a plane perpendicular to the plane of the macrocycles.

We have used the experimental geometry of PcFe in the monomers and polymers. Furthermore, we take the distance Fe–N (bridged ligands) at 2.0 Å, according to experimental data for similar systems [71–73]. We have optimized the geometry of the bridged ligands, using the ADF code. The resulting geometries are used in the calculations of monomers and polymers.

Results and Discussion

PHTHALOCYANOIRON GROUND-STATE ELECTRONIC STRUCTURE

Before describing the metal–bridged ligand interaction, it is necessary to show the changes that occur when the Fe^{2+} is inserted in the phthalocyanine macrocycle, Pc^{2-}. We show in Figure 4 the

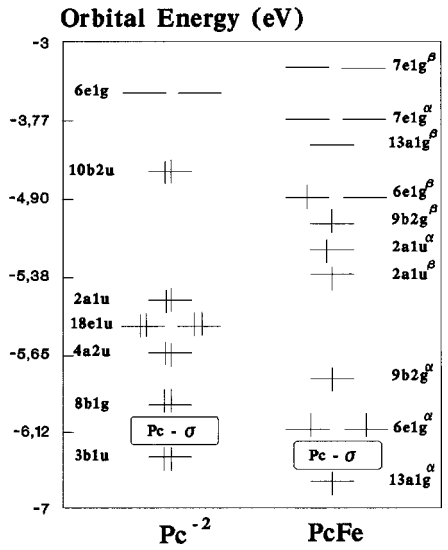

FIGURE 4. Energy level scheme for Pc^{2-} (spin restricted) and PcFe (spin unrestricted).

one-electron levels obtained by the spin unrestricted calculation for PcFe, together with the levels of the Pc^{2-}. A D_{4h} symmetry was used. The Pc^{2-} levels have been rigidly shifted by 5.3 eV to lower energies in order to bring the $2a_{1u}$ levels as a reference to evaluate the perturbation effects induced the by metal. The ground state of PcFe is ^3E_g. The occupations of the one-electron levels are indicated in Figure 4. For a discussion of the trends in the one-electron energies, it is instructive to look at the composition of the individual orbitals. In Table I the composition of the most important orbitals are given in terms of Fe and Pc orbitals.

The increasing energy level order of the metal orbitals, $d_{x^2-y^2} > d_{xy} > d\pi(d_{xz}, d_{yz}) > d_{z^2}$ is in agreement with Goutermen's calculation [74–77]. The level $2a_{1u}$ of the Pc^{2-} is found in the frontier region between d_{xy} and $d\pi$ metal orbitals. The electronic ground-state configuration $(d_{xy})^2(d\pi)^3(d_{z^2})^1$ is the same given by Coppen's charge density determinations, using X-ray data [78, 79], where a double occupation for d_{xy} is suggested. The same occupation was proposed earlier by Gouterman et al. The LUMO is $13A_{1g}^{\beta}$ The LUMO+1 orbitals, $7e_g(\pi^*)$, come from an interaction between $d\pi$ of metal and $6e_g(\pi^*)$ of the Pc^{2-}.

PcFe–L_2 COMPLEXES

Orbital Interactions

The introduction of axial ligands modifies the Phthalocyanoiron (PcFe) ground-state electronic

TABLE I

Percent contribution of Pc and Fe fragments to selected orbitals (based on Mulliken population analysis per MO) of phthalocyanoiron, where only the main contributions to each orbital have been given.

	ε (eV)	Fe	Pc
$13a_{1g}^{\beta}$	−4.351	86 (d_{z^2}, 4s)	14 ($11a_{1g}$)
$6e_{1g}^{\beta}$	−4.904	64 ($d\pi$)	36 ($5e_{1g}$)
$6b_{2g}^{\beta}$	−5.076	84 (d_{xy})	16 ($8b_{2g}$, $10b_{2g}$)
$2a_{1u}^{\alpha}$	−5.372	0	100 ($2a_{1u}$)
$2a_{1u}^{\beta}$	−5.382	0	100 ($2a_{1u}$)
$9b_{2g}^{\alpha}$	−5.862	53 (d_{xy})	47 ($8b_{2g}$, $10b_{2g}$)
$6e_{1g}^{\alpha}$	−6.121	47 ($d\pi$)	53 ($5e_{1g}$)
$13a_{1g}^{\alpha}$	−6.918	84 (d_{z^2})	16 ($11a_{1g}$)

configuration described in the previous section. Experimental evidence confirm a low-spin pseudo-octahedral Fe(II) environment in PcFe–L_2 complexes as well as $[PcFe–L]_n$ polymers [80–82]. Furthermore, these compounds show an electron spin resonanse (ESR) silent sign, associated with a restricted electronic state [82]. We have used this electronic state to study the PcFe–L_2 complexes with L = py, pyz, tri, tz, bpy, acpy, and bybe.

We found that in all the studied complexes, axial ligands prefer to be located toward the aza nitrogen atoms of PcFe. In Figure 5 is shown the

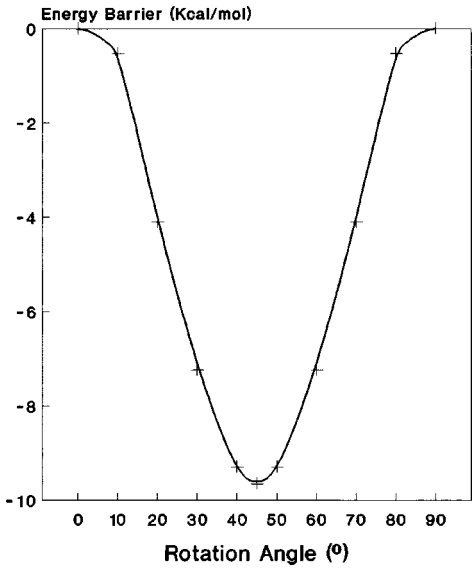

FIGURE 5. Energy barrier profile for the rotation angle of pyz in the PcFe–py_2 complex.

TABLE II

Energetic barrier ($\Delta E_{barrier}$ kcal/mol) upon variation of the rotation angle of the axial ligand from 0° to 45°.

Complex	$\Delta E_{barrier}$ (kcal/mol)
PcFe–pyz_2	−9.655
PcFe–tri_2	−9.036
PcFe–tz_2	−7.334
PcFe–py_2	−9.107
PcFe–bpy_2	−8.147
PcFe–$acpy_2$	−8.158
PcFe–$bybe_2$	−8.114

energy barrier that exists when the pyrazine goes from a position pointing to the pyrrolic nitrogenous (N_p, 0°) toward the position pointing to the aza nitrogenous (N_a, 45°) and thereafter going to the next pyrrolic nitrogen (90°). In Table II, we summarize the energy barrier described above for the set of ligands. This result is in agreement with the crystalline structures determined for some ligands [71–73]. In the next section, we will try to find an explanation for this result.

In Figure 6, the ground-state one-electron levels are shown for the series PcFe–L_2 with L = py, pyz, tri, tz, bpy, acpy, and bybe. For some selected complexes and their molecular orbitals, an atomic orbital population analysis is given in Table III. The monomers show different symmetry labels: PcFe–L_2 with py, pyz, bpy, acpy, and bybe have a D_{2h} symmetry. For L = tri and tz, the symmetry became C_{2v}. For brevity, we will describe the frontier orbital of monomers PcFe–L_2 with L = pyz and tz. This is due to the fact that the results with pyz are similar to those obtained for py, bpy, azpy, and bybe. On the other hand, the result with tz is similar to that obtained with tri.

As expected for PcFe, the d_{z^2} orbital is highly destabilized though the σ-interaction with the HOMO of the bridged ligands. The d_{z^2} orbital remains empty. Furthermore, the π-donation destabilization of the $d(\pi)$ orbitals (d_{xz} and d_{yz}), even though not as pronounced as that of the d_{z^2} orbital, appears to be strong enough to increase the backbonding from the metal to the LUMO, which has a high contribution from the macrocycle ring. This interaction is expected to decrease the reducing capability of the metal center.

As mentioned before, the main interest of this study resides in the electronic properties. Therefore, we analyzed the highest occupied and the lowest unoccupied molecular orbitals. In the monomers, the HOMO is a d_{xy} of transition metal. This orbital is practically fixed in energy for the set of axial ligands (see Fig. 6).

With respect to LUMO, when the [PcFe$(pyz)_2$] monomer is formed, such an orbital arises from the interaction between one metallomacrocycle π^*

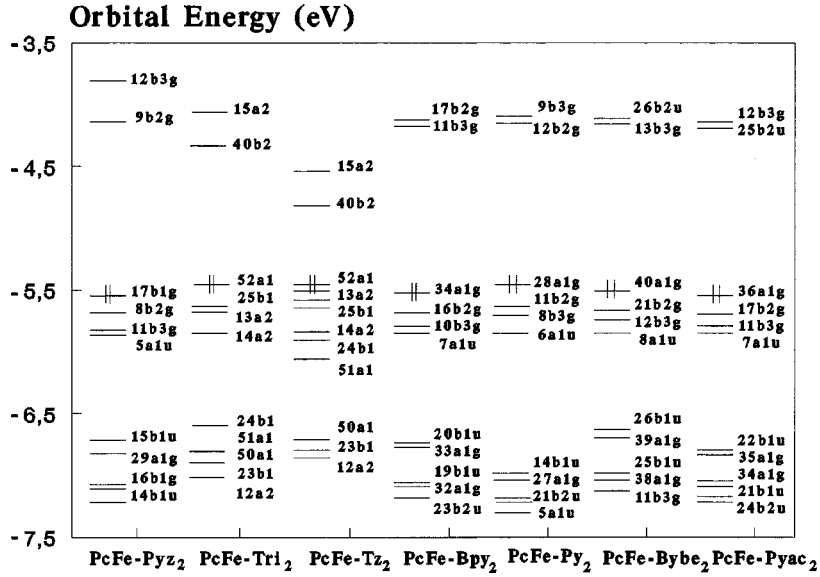

FIGURE 6. Energy level frontier for the PcFe–L_2 complexes with L = pyz, tri, tz, py, bpy, bpyac, and bybe. All lower lying orbitals are also doubly occupied.

TABLE III

Percentage contribution of individual fragments to selected orbitals (based on Mulliken population analysis per MO) of PcFe–L_2 with L = pyz, tri, tz, bpy, and py.

PcFe–pyz_2 ε (eV)	−3.81	−4.14	−5.54 (HOMO)	−5.69	−5.82	−5.84	−6.71
Orbital symmetry	$22b_{3g}$	$9b_{2g}$	$17b_{1g}$	$8b_{2g}$	$11b_{3g}$	$5a_{1u}$	$15b_{1u}$
Fe	0.00	4.30	84.0 (d_{xy})	64.0 (d_{xz})	71.0 (d_{yz})	1.00	0.00
Pc	0.00	80.7	16.0	36.0	29.0	99.0	0.00
Pyz	100	15.0	0.00	0.00	0.00	0.00	100
PcFe–Tri_2 ε (eV)	−4.06	−4.33	−5.45 (HOMO)	−5.62	−5.64	−5.84	−6.59
Orbital symmetry	$15a_2$	$40b_2$	$52a_1$	$25b_1$	$13a_2$	$14a_2$	$24b_1$
Fe	7.10	0.00	81.4 (d_{xy})	68.6 (d_{xz})	69.0 (d_{yz})	2.00	0.00
Pc	7.90	0.00	18.6	31.4	31.0	98.0	0.00
Tri	85.0	100	0.00	0.00	0.00	0.00	100
PcFe–Tz_2 ε (eV)	−4.54	−4.82	−5.45 (HOMO)	−5.48	−5.58	−5.84	−6.07
Orbital symmetry	$15a_{u2}$	$40b_2$	$52a_1$	$13a_2$	$25b_1$	$14a_2$	$24b_1$
Fe	13.9	0.00	77.9 (d_{xy})	68.0 (d_{yz})	62.4 (d_{xz})	1.00	0.00
Pc	0.00	0.00	22.1	32.0	37.6	99.0	0.00
Tz	86.1	100	0.00	0.00	0.00	0.00	100
PcFe–Bpy_2 ε (eV)	−4.11	−4.12	−5.53 (HOMO)	−5.69	−5.78	−5.84	−6.77
Orbital symmetry	$17b_{2g}$	$11b_{3g}$	$34a_{1g}$	$16b_{2g}$	$10b_{3g}$	$7a_{1u}$	$20b_{1u}$
Fe	10.3	8.50	83.9 (d_{xy})	69.7 (d_{xz})	62.9 (d_{yz})	0.00	0.00
Pc	89.7	91.5	16.1	30.3	23.5	100	0.00
Bpy	0.00	0.00	0.00	0.00	8.69	0.00	100
PcFe–Py_2 ε (eV)	−4.09	−4.10	−5.47 (HOMO)	−5.63	−5.71	−5.84	−7.00
Orbital symmetry	$9b_{3g}$	$12b_{2g}$	$28a_{1g}$	$11b_{2g}$	$8b_{3g}$	$6a_{1u}$	$14b_{1u}$
Fe	11.4	11.1	84.7 (d_{xy})	70.0 (d_{xz})	64.9 (d_{yz})	0.00	0.00
Pc	88.6	88.9	7.71	30.0	24.1	100	2.70
Py	0.00	0.00	0.00	0.00	10.9	0.00	97.3

orbital and pyrazine ligand π^* orbital. Both have b_{2g} symmetry. This interaction has no direct energetic consequences, since the bonding combination is unoccupied ($9b_{2g}$). The LUMO orbital, $9b_{2g}$, shows the following composition: 85% from the π^* system PcFe and 15% from π^* pyrazine ligand. In contrast, when the bridged ligand is tetrazine, the LUMO orbital in [PcFe$(tz)_2$] is 100% formed by π^* system of such a ligand. This is a nonbonding orbital. However, the HOMO–LUMO gap is considerably smaller than the system with pyz, when it is used as a bridging ligand. This description confirms the best semiconduction properties associated to the tetrazine as ligand.

We have calculated the hardness of the complexes studied from Eq. (4). The results are summarized in Table IV. The smaller the hardness value, the better will be the semiconduction. Furthermore, when the number of nitrogen atoms in the axial ligand increases (for example, pyz to tz), the semiconduction is enhanced. This is due to the fact that a nitrogen atom is more electronegative than the —CH group, producing a greater stabilization of the ligand's LUMO, and therefore a reduction in the HOMO–LUMO gap. This is in agreement with the second-order perturbation theory at electronegativity level [83].

TABLE IV

Hardness results for PcFe–L_2 complexes.[a]

Complex	LUMO	HOMO	η
PcFe–pyz_2	−4.126	−5.542	1.412
PcFe–tri_2	−4.325	−5.453	1.128
PcFe–tz_2	−4.817	−5.453	0.636
PcFe–py_2	−4.101	−5.465	1.364
PcFe–bpy_2	−4.117	−5.525	1.408
PcFe–$bybe_2$	−4.113	−5.506	1.394
PcFe–$bpyac_2$	−4.182	−5.537	1.356

[a] Energies in eV.

Energy Decomposition

We will try of explain why axial ligands prefer to be located toward the aza nitrogen atoms of PcFe. To achieve this, we decompose the bonding energy in the rotation of the ligand from 0° to 45° (conformation more stable) keeping the Fe–N (ligand) distance fixed at 2 Å. A comparison between the interaction diagrams for the two possible conformations of the axial ligands show that these interactions are enhanced in the conformation at 0°, compared to the conformation at 45° (see Fig. 7). It should be noted that most of these interactions involve orbitals and have been referred in the discussion of computational details and geometrical parameters above as four-electron two-orbital repulsion. The results of this analysis are shown in Table V. According to the data reported in the third column of Table V, a rotation of 45° of the axial ligands induces on the complexes series a decrease of about 3.6% average in the attractive electrostatic interaction ΔE_{elstat}. These can be explained since a 45° conformation increases the distances between most of the atoms of the two interacting fragments in such a way that the stabilizing interactions between the charge density of one fragment with the nuclei of the other fragment decreases. Looking at the Pauli repulsion term, ΔE_{Pauli}, we notice that this term is reduced by about 2.6% average, upon variation of the rotation angle from 0° to 45°. This could be understood in terms of a decrease of the overlap between most of the occupied orbitals on the interacting fragments. The Pauli repulsion term is highly positive in all the complexes. It should be noted that although the Pauli repulsion decreases when the axial ligands are in a conformation of 45°, it still remains strong.

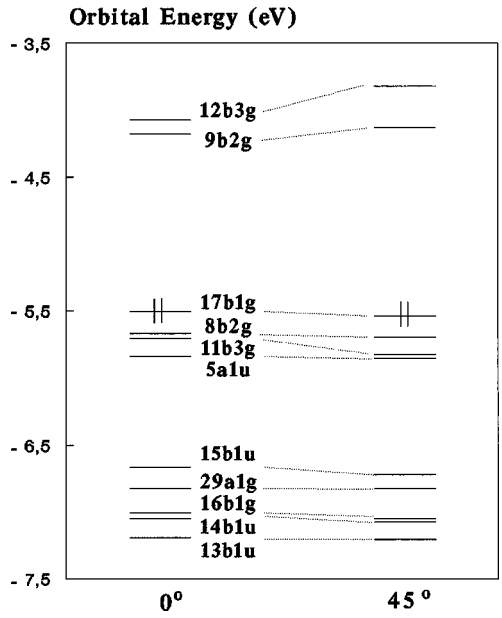

FIGURE 7. Energy level scheme for PcFe–pyz_2 to 0° and 45° angle of pyz in the metallomacrocycle. All lower lying orbitals are also doubly occupied.

TABLE V
Contributions (eV) to the bonding energy of PcFe–L_2 complexes.

Complex	ϕ	ΔE_{elstat}	ΔE_{Pauli}	ΔE^0	ΔE_{i0}	ΔE_{total}
PcFe–pyz_2	0°	−12.977	33.075	20.098	−23.038	−2.941
	45°	−12.473	32.254	19.781	−23.145	−3.364
PcFe–tri_2	0°	−11.002	32.329	21.327	−24.110	−2.783
	45°	−10.694	31 .790	21.096	−24.270	−3.175
PcFe–tz_2	0°	−10.534	31.357	20.823	−23.724	−2.901
	45°	−10.280	30.893	20.613	−23.831	−3.220
PcFe–py_2	0°	−12.545	37.360	24.815	−27.189	−2.375
	45°	−12.048	36.443	24.395	−27.164	−2.768
PcFe–bpy_2	0°	−12.411	36.999	24.588	−26.825	−2.240
	45°	−11.904	36.090	24.186	−26.779	−2.593
PcFe–$acpy_2$	0°	−12.413	36.974	24.561	−26.791	−2.230
	45°	−11.904	36.063	24.159	−26.742	−2.583
PcFe-$bybe_2$	0°	−12.421	37.027	24.606	−26.884	−2.278
	45°	−11.912	36.116	24.204	−26.833	−2.630

Both ΔE_{Pauli} and ΔE_{elstat} change in appositive directions upon changing the rotation angle, but ΔE_{Pauli} is larger in absolute terms and has a larger variation. Thus, when ΔE_{Pauli} and ΔE_{elstat} are combined into the steric interaction energy (ΔE^0) one finds that ΔE^0 is destabilizing (positive), both for the 0° and 45° configurations, but is smaller for the last. As far as the stabilizing orbital interaction term ΔE_{0i} is concerned, we first notice that it is little influenced by the variation of axial ligands, and second, it gives the stabilizing contribution for each conformation, but it is rather insensitive to the change of the ligand groups.

From Table V, it can be appreciated that the steric repulsion dominates the attractive occupied/virtual orbital interaction upon variation of the rotation angle from 0° to 45°. We have therefore clearly identified the Pauli repulsion as the origin of the configuration at 45° with respect to the axial ligands as the more stable conformation.

$[PcFe(L)]_n$ POLYMERS

When going from the complex to the infinite chain, due to the stacked effects of PcFe units, we would have to expect a smaller band gap. We used pyz and tz as modes for this study. Table VI shows such an effect for the systems with pyz and tz in dimers and polymers, respectively. The band gap is significantly reduced once the polymer is built.

We are going to describe the frontier band structures for the —$[PcFe(L)]_n$ with L = pyz, tz. Thereafter, we will make a generalization of the results found for the rest of the polymers. Only the highest occupied frontier crystal orbitals (CO) and the two lowest unoccupied CO (LUCO) are shown in the range −7 to −4.3 eV in Figures 8(a) and 8(b). There are several flat bands that correspond to well-localized electrons. For simplicity, we continue using the symmetry of the complexes in the polymers. Among them, we found that the bands fall in the −5.5- to −6.0-eV range, which is associated to the highest occupied crystal orbital (HOCO) cor-

TABLE VI
Summary of results[a] for —$[PcFe(pyz)]_n$ (i), —$[PcFe(tz)]_n$ (ii), $[PcFe(pyz)_2]$ (iii), and $[PcFe(tz)_2]$ (iv).

	i[e]	ii[e]	iii	iv
HOMO[b]	−5.542	−5.453	−5.542	−5.543
LUMO[c]	−4.902	−5.357	−4.126	−4.817
Gap[d]	0.640	0.096	1.412	0.636

[a] Energy in eV.
[b] Highest occupied molecular orbital.
[c] Lowest unoccupied molecular orbital.
[d] Transition energy between the HOMO and the LUMO.
[e] For polymers i and ii, the corresponding terms are HOCO, LUCO, and band gap.

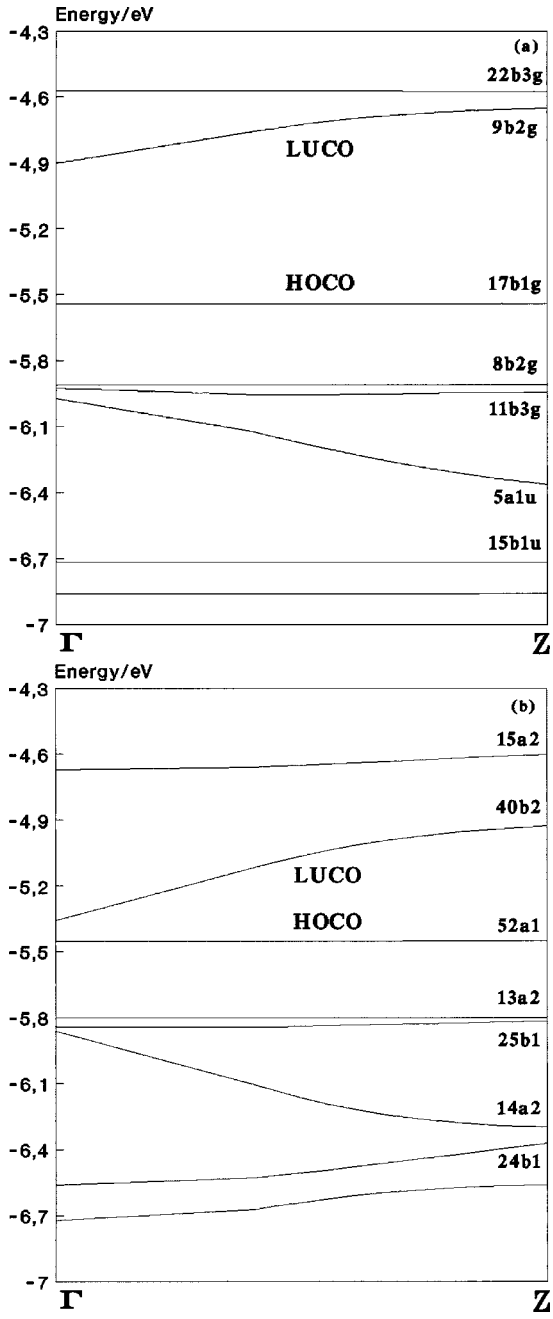

FIGURE 8. Band structures for (a) [PcFe–pyz]$_n$ and (b) [PcFe–tz]$_n$.

TABLE VII
Summary of computational results[a] for the —[PcFe(L)]$_n$ polymers.[b]

Polymer	LUCO[c]	HOCO[d]	Band gap theoretical[e]	Band gap experimental	σ
—[PcFe(pyz)]$_n$	−4.902	−5.542	0.640	0.80	1×10^{-6}
—[PcFe(tri)]$_n$	−5.053	−5.453	0.399		7×10^{-6}
—[PcFe(tz)]$_n$	−5.357	−5.453	0.096	0.10	1×10^{-1}
—[PcFe(bpy)]$_n$	−4.717	−5.525	0.808	1.44	2×10^{-8}
—[PcFe(bpyac)]$_n$	−4.773	−5.537	0.764		1×10^{-7}

[a] Energy in eV.
[b] Experimental energy gaps and conductivity (σ, S/cm) [8–27].
[c] Lowest unoccupied crystal orbital.
[d] Highest occupied crystal orbital.
[e] Transtion energy between the HOCO and the LUCO.

responding to d_{xy} and the π-bands of the Fe atom. Besides, we have found in this range a band with a quite dispersed, with $5a_{1u}$ and $14a_2$ symmetry corresponding to Pc in the systems —[PcFe–pyz]$_n$ and —[PcFe–tz]$_n$, respectively.

A different situation is appreciated in the conduction band corresponding to the LUCO. Let's write out the Bloch functions at the center ($k = 0$, Γ) and edge ($k = \pi/a$, Z) of the Brillouin zone. The LUCO band for the polymers runs up toward Z vector, which in turn corresponds to the most antibonding combination. The composition of this band is very similar to that shown by the monomer. Thus, the polymer with pyz shows a composition that is 85% PcFe and a 15% bridging ligand; while with tz, the composition is 100% formed by π^* system of such a ligand.

In Table VII, we have summarized the results for all polymers including experimental measures [8–27]. The metallomacrocycle polymers with bridged ligands showed semiconducting properties in agreement with the experimental measurements of energy gap. It is interesting to note that our predicted band gap, agrees with the experimental condictivity and with the available estimation of the band gap.

We have also built the density of states (DOS) [84, 85] and its projection on the Fe and bridged ligands. The DOS show the behaviors described in the band structures for the [PcFe(L)]$_n$ (L = pyz, tz) systems (Fig. 9). The projections of the metal and bridged ligand orbitals in the density of states showed mainly a metal character in the valence band (VB) near the Fermi level, and the ligand participation in the conduction band (CB). Independently of the polymer, both the HOCO and LUCO bands are very similar to those of the monomeric units described previously.

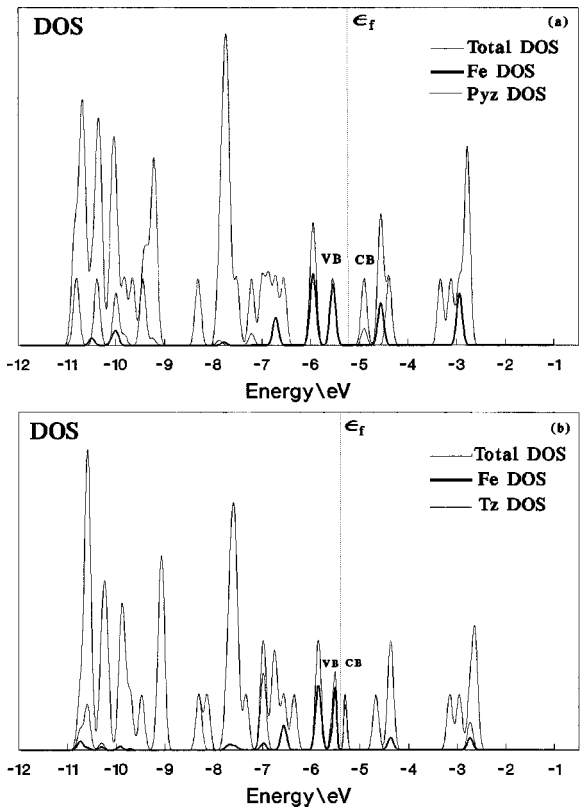

FIGURE 9. Density of states for [PcFe–L]$_n$ polymers with the projections Fe, pyz, and tz, which illustrate the nature of the frontier crystal orbital: (a) [PcFe–pyz]$_n$ and (b) [PcFe–tz]$_n$.

Conclusions

The analysis of the electronic structures of the polymers and complexes indicate that: (i) the HOCO is very flat band, largely composed of the transition metal orbitals (approximately 85%) with some contribution of the ring orbitals. (ii) The LUCO band is composed of a mixture between the ring and bridged ligand orbitals, as in the case of the systems formed by pyz, bpy, and bpyac. This composition is completely different when the ligand is tri and tz. Such a band is exclusively composed of the π system of tri and tz. Thus, these systems showed the highest conductivity of the polymer studied here.

ACKNOWLEDGMENTS

This work was supported by FONDECYT Project No. 1990038. Also, the authors thank Dr. Luis Padilla (Comisión Chilena de Energía Nuclear) for the access to the ADF 2.3 version package.

References

1. Kellog, G. E.; Gaudiello, J. G. In Polymeric Coordination Camplexes: Bridging Molecular Metals and Conductive Polymers. Inorganic Materials; Bruce, D. W.; O'Hare, D., Eds.; Wiley: New York, 1992, pp. 353–404.
2. Zeldin, M.; Wynne, K. J.; Allcock, H. R. In Inorganic and Organometallic Polymers; ACS Symposium Series, Vol. 360; ACS: Washington DC, 1988.
3. Cassoux, P.; Valade, L. Molecular Inorganic Superconductos, Inorganic Materials; Bruce, D. W.; O'Hare, D., Eds.; Wiley: New York, 1992; pp. 1–58.
4. Rosenblum, M. Adv Mater 1996, 6, 159.
5. Böhm, M. C. In One-Dimensional Organometallic Materials; Lectures Notes in Chemistry, No. 4; Springer: 1988.
6. Deger, S.; Lange, A.; Hanack, M. Chem Coord Rev 1988, 83, 115.
7. Marks, T. Science 1995, 227, 881.
8. Schultz, H.; Lehmann, H.; Rein, M.; Hanack, M. Structure and Bonding 1991, 74, 41.
9. Hanack, M. Macromol Symp 1994, 80, 83.
10. Hanack, M.; Lang, M. Adv Mater 1994, 6, 819.
11. Hanack, M. GIT Fachz Lab 1987, 2, 75.
12. Fernandez, F.; Torres, T.; Hauschel, B.; Hanack, M. Chem Rev 1998, 98, 563.
13. Bryce, M. R. Chem Br 1988, 781.
14. Chen, C.-T.; Suslick, K. S. Coord Chem Rev 1993, 128, 193.
15. Hanack, M.; Knecht, S.; Schulte, M. J Organometallic Chem 1993, 445, 157.
16. Knecht, S.; Polley, R. Chem Ber 1995, 128, 928.
17. Pohmer, J.; Hanack, M.; Barcina, J. J Mater Chem 1996, 6, 957.
18. Kang, Y. G.; Kim, H. Synth Met 1997, 78, 11.
19. Hanack, M.; Lange, A.; Grosshans, R. Synth Met 1991, 45, 59.
20. Hanack, M.; Hedmann-Rein, C.; Münz, X. Synth Met 1987, 19, 787.
21. Kleinwachter, J.; Hanack, M. J Am Chem Soc 1997, 119, 10684.
22. Hanack, M.; Fischer, K. Synth Met 1985, 10, 345.
23. Ziener, U.; Fahmy, N.; Hanack, M. Chem Ber 1996, 126, 2559.
24. Bulatov, A.; Knecht, S.; Subramaian, L. R. Chem Ber 1993, 126, 2565.
25. Hanack, M.; Polley, R. Inorg Chem 1994, 33, 3201.
26. Collman, J. P.; McDevitt, J. T.; Leidner, C. R. J Am Chem Soc 1987, 109, 4606.
27. Hiller, R.; Hanack, M.; Mezgar, M. Acta Cryst C 1987, 43, 1264.
28. Hanack, M.; Gül, A.; Subramanian, L. R. Inorg Chem 1992, 31, 1542.
29. Keppler, U.; Deger, S.; Lange, A.; Hanack, M. Angew Chem Int Ed Engl 1987, 26, 724.
30. Diel, B. N.; Inabe, T.; Jaggi, N. K.; Lyding, J. W.; Schneider, O.; Hanack, M.; Kannewurf, C. R.; Marks, T. J.; Schwartz, L. H. J Am Chem Soc 1984, 106, 3207.
31. Kleinwächter, J.; Hanack, M. J Am Chem Soc 1997, 119, 10684.
32. Gaudillo, J. G.; Kellogg, G. E.; Tetrick, S. M.; Marks, T. J. J Am Chem Soc 1989, 111, 5259.
33. Hanack, M.; Schlick, U. Inorg Chem 1995, 34, 3621.
34. Schneider, O.; Hanack, M. Chem Ber 1983, 116, 2088.
35. Meier, H.; Albrecht, W.; Zimmerhackl, E.; Hanack, M.; Metz, J. J Synth Met 1985, 11, 333.
36. Meier, H.; Albrecht, W.; Hanack, M.; Koch, J. Polymer Bull 1986, 16, 75.
37. van Nostrum, C. F.; Nolte, R. J. Chem Commun 1996, 2385.
38. Wang, H.-H.; Williams, J. M.; Whangbo, M.-H. Synth Met 1991, 41, 1983.
39. Whangbo, M.-H.; Stewart, K. R. Isr J Chem 1983, 23, 133.
40. Canadell, E.; Alvarez, S. Inorg Chem 1984, 23, 573.
41. Baerends, E. J.; Ellis, D. E.; Ros, P. Chem Phys 1973, 2, 42.
42. Baerends, E. J.; Ros, P. Int J Quantum Chem 1978, S12, 169.
43. te Velde, G.; Baerends, E. J. Phys Rev B 1991, 44, 7888.
44. Becke, A. D. J Chem Phys 1986, 84, 4524.
45. Stoll, H.; Golka, E.; Preuss, E. Theor Chim Acta 1980, 29, 55.
46. Vosko, S. H.; Wilk, L.; Nusair, M. J. Can J Phys 1980, 58, 1200.
47. Rosa, A.; Baerends, E. J. Inorg Chem 1992, 31, 4717.
48. Rosa, A.; Baerends, E. J. Inorg Chem 1993, 32, 5637.
49. Rosa, A.; Baerends, E. J. Inorg Chem 1994, 33, 584.
50. Snijders, J. G.; Vernooijs, P.; Baerends, E. J. At Data Nucl Data Tables 1982, 26, 483.
51. Morokuma, K. Acc Chem Res 1977, 10, 294.
52. Ziegler, T.; Rauk, A. Inorg Chem 1979, 18, 1558.
53. Ziegler, T.; Rauk, A. Inorg Chem 1979, 18, 1755.
54. Fujimoto, H.; Osamura, J.; Minato, T. J Am Chem Soc 1978, 100, 2954.
55. Kitaura, K.; Morokuma, K. Int J Quantum Chem 1976, 10, 325.

56. Ziegler, T.; Rauk, A. Theor Chim Acta 1977, 46, 1.
57. Parr, R. G.; Yang, W. In Density Functional Theory of Atoms and Molecules; Oxford University Press: New York, 1989.
58. Kohn, W.; Becke, A. D.; Parr, R. J Phys Chem 1996, 100, 12974.
59. Parr, R. G.; Donnelly, R. A.; Levy, M.; Palke, W. E. J Chem Phys 1978, 68, 3801.
60. Pearson, R. G. Acc Chem Res 1993, 26, 250.
61. Person, R. G. In Chemical Hardness; Wiley-VCH: 1997.
62. Koopman, T. A. Physica 1933, 1, 104.
63. Parr, R. G.; Zhou, Z. Acc Chem Res 1993, 26, 256.
64. Mendizabal, F.; Contreras, R.; Aizman, A. Int J Quantum Chem 1995, 56, 820.
65. Mendizabal, F.; Contreras, R.; Aizman, A. J Phys Condens Matter 1997, 9, 3011.
66. Kirner, J. F.; Dow, W.; Scheidt, R. W. Inorg Chem 1976, 15, 1685.
67. Metz, J.; Schneider, O.; Hanack, M. Spectrochim Acta 1982, 1265.
68. Hanack, M.; Keppeler, U.; Lange, M.; Irsch, A.; Dieing, R. In Phthalocyanines, Properties and Applications; Leznoff, C. C.; Lever, A. B. P., Eds.; VCH: Weinheim, 1993; Vol. 2.
69. Keppeler, U.; Kobel, W.; Siehl, H.-U.; Hanack, M. Chem Ber 1985, 118, 2095.
70. Aldinger, R.; Hanack, M.; Herrmann, K.; Hirsch, A.; Kasper, K. Synth Met 1993, 60, 265.
71. Hanack, M.; Mezger, M.; Hiller, W. Acta Crystallogr C 1987, 43, 1264.
72. Kubel, F.; Strähle, J. Z. Naturforsch Teil B 1981, 36, 441.
73. Hedtmann-Rein, C.; Hanack, M.; Peters, K.; Peters, E.; von Schnering, H. Inorg Chem 1987, 26, 2647.
74. Schaffe, A. M.; Gouterman, M.; Davidson, E. R. Theor Chim Acta 1973, 30, 9.
75. Tatsumi, K.; Hoffmann, R. J Am Chem Soc 1981, 103, 3328.
76. Sontum, S. F.; Case, D. A. J Am Chem Soc 1985, 107, 4013.
77. Fierro, C.; Anderson, A. B.; Scherson, D. A. J Phys Chem 1988, 92, 6902.
78. Coppens, P.; Liang, L.; Zhu, N. J. J Am Chem Soc 1983, 105, 6173.
79. Lever, A. B. P. J Chem Soc 1965, 1821.
80. Keppeler, U.; Deger, S.; Lange, A.; Hanack, M. Angew Chem 1987, 99, 349.
81. Wei, H.-H.; Shyu, H.-L. Polyhedron 1985, 4, 979.
82. Ouédraogo, G. V.; More, G. C.; Richard, Y.; Benlian, D. Inorg Chem 1981, 20, 4387.
83. Albright, A. T.; Burdett, J. K.; Whangbo, M.-H. In Orbital Interactions in Chemistry; Wiley: New York, 1985.
84. Yu, H. L. Phys Rev B 1977, 15, 3609.
85. Arratia-Perez, R. Chem Phys Lett 1993, 213, 547.